

Features of ion acceleration by circularly polarized laser pulses

T. V. Liseykina

*Dipartimento di Fisica “E. Fermi”, Università di Pisa, Pisa, Italy**

A. Macchi

polyLAB, CNR-INFM, Università di Pisa, Pisa, Italy†

(Dated: November 1, 2018)

The characteristics of a MeV ion source driven by superintense, ultrashort laser pulses with circular polarization are studied by means of particle-in-cell simulations. Predicted features include high efficiency, large ion density, low divergence and the possibility of femtosecond duration. A comparison with the case of linearly polarized pulses is made.

The short-duration, multi-MeV ion beams produced in the interaction of high-intensity laser pulses with solid targets have proven to be effective for applications such as proton radiography,^{1,2} diagnostic of highly transient electromagnetic fields,^{2,3,4} isochoric heating of matter,⁵ isotope production⁶ and nuclear activation.⁷ Foreseen future applications to medicine,⁸ nuclear fusion⁹ or particle physics¹⁰ will require improvements in factors such as the conversion efficiency, peak ion energy, beam monochromaticity and collimation. Recent experiments performed with these aims^{11,12,13} are based on the target normal sheath acceleration (TNSA) mechanism,¹⁴ where ions on a surface layer at the rear side of the target are accelerated by the space-charge field of escaping “fast” electrons. Numerical simulations have also explored different regimes, such as “shock acceleration”,¹⁵ “laser-piston”,¹⁶ “skin-layer ponderomotive acceleration”,¹⁷ or acceleration by circularly polarized laser pulses,¹⁸ where as a common feature ion acceleration occurs at the target front side and is in principle dominated by the effect of the radiation pressure of the laser pulse. These regimes might be the leading ones at ultra-high intensities¹⁶ or be most suitable for specific applications.¹⁷

Here we report a numerical study on ion acceleration with circularly polarized pulses (CP) with the aim to show the peculiar features of the ion source (high efficiency, large ion density, short duration, good collimation) which may be advantageous for specific applications. A comparison with the case of linearly polarized pulses (LP) is made to evidenciate the differences with CP and to provide a deeper understanding of “ponderomotive” (i.e. radiation pressure-dominated) mechanisms. This is possible because using CP at normal incidence fast electron generation is almost suppressed,¹⁸ thus related effects (such as TNSA) can be separated by purely ponderomotive ones.

We compare two one-dimensional (1D) particle-in-cell (PIC) simulations performed for LP and CP, respectively, and having same pulse wavelength ($\lambda_L = 1 \mu\text{m}$), duration ($\tau_L = 26T_L = 86 \text{ fs}$ where $T_L = \lambda_L/c$), and intensity $I = 3.5 \times 10^{20} \text{ W cm}^{-2}$. To ensure that I is the same, the peak field amplitude in the CP case, $a_L = 11.3$, is lower by a factor $\sqrt{2}$ than in the LP case $a_L = 16$. Here, a_L is the dimensionless pulse amplitude given by

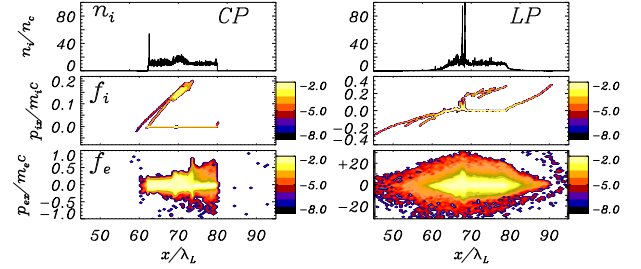


FIG. 1: Snapshots at $t = 140T_L = 467 \text{ fs}$ of the ion density n_i (top) and the (x, p_x) phase space projections of ions (f_i , middle) and electrons (f_e , bottom) from 1D PIC simulations in the CP (left) and LP (right) cases. The laser pulse propagates from left to right. Length scales are normalized to $\lambda_L = 1 \mu\text{m}$, the density to n_c , and momenta to mc . Notice the different scale on the momentum axes between the CP and LP cases.

$a_L = 0.85\sqrt{(I\lambda^2)_{18}/\alpha}$ where $(I\lambda^2)_{18}$ is the irradiance in units of $10^{18} \text{ W cm}^{-2}$ and $\alpha = 1$ (2) for LP (CP). The plasma parameters are the same for both simulations (proton plasma slab of $20 \mu\text{m}$ thickness and electron density $n_e = 10n_c$ where $n_c = 1.1 \times 10^{21} \text{ cm}^{-3}$ is the cut-off density). The parameters of the LP case are close to those of simulations reported by Silva et al.¹⁵ to address “shock” acceleration. In both our simulations, the temporal and spatial resolution were given by $\Delta x = c\Delta t = \lambda_L/400$ and 32 particles per cell were used. The high spatio-temporal resolution was necessary to ensure convergence of the results, since very sharp gradients are generated during the interaction, e.g. at the ion density spiking discussed below and elsewhere.^{18,19}

Fig.1 compares the ion density profiles and the phase space of ions and electrons for CP and LP. For LP, strongly relativistic electrons with momenta p_{ex} up to $\simeq 30m_e c$ are generated. The ion phase space shows at least three “groups”: ions accelerated by TNSA both at the front and the rear side, with momenta p_{ix} up to $\simeq 0.3m_e c$, and ions accelerated at the front surface propagating into the plasma with similar momentum values. For CP, electrons are relatively “cold”, since typical momenta are more than one order of magnitude lower than for LP. No significant TNSA ions are observed, and most

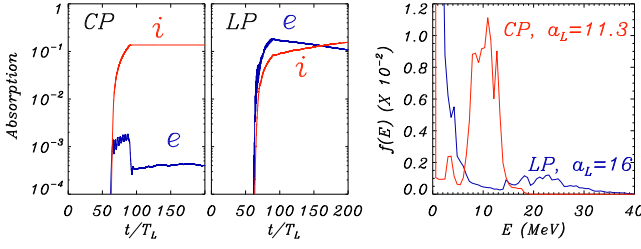


FIG. 2: Comparison of absorption efficiency into ions and electrons vs. time (left) and of ion energy spectra (right) from 1D PIC simulations of ion acceleration with LP or CP pulses for the same plasma parameters and laser energy and duration.

of the accelerated ions are located in a bunch with longitudinal momentum $p_x \simeq 0.15m_i c$.

Fig.2 compares the absorption efficiency and the ion spectrum obtained in the CP and LP cases, respectively. The absorption into bunch ions is 13.7% for CP and is constant after the laser pulse, confirming that all ions are “directly” accelerated ponderomotively; absorption into electrons is negligible. For LP, absorption into electrons is dominant during the interaction with the laser pulse; later, energy transfer towards ions occurs and the conversion efficiency into ion energy has a value similar to CP, but including all the three ion groups observed in Fig.1. The ion spectrum for CP is relatively narrow and peaked around 10 MeV, while the LP spectrum is more thermal-like, with a broad maximum around 20 MeV.

While ponderomotive acceleration (PA) is the only effective ion acceleration channel in the CP case, for LP its contribution overlaps with TNSA, and the same analytical model proposed for the CP case¹⁸ may be used if the longitudinal force on ions is considered to be a temporal average. the forward accelerated ions at the front surface observed for LP may be attributed to PA (rather than to “shock” acceleration¹⁵), and the same model. However, the strong absorption into electrons for LP reduces the total radiation pressure and so the PA efficiency. An estimate of the relative contributions of TNSA and PA is provided by an analysis of particle energy vs. position, showing that at the time corresponding to Fig.1 the energy belonging to ions located within the original plasma slab position ($60 \mu\text{m} < x < 80 \mu\text{m}$) is 76% of the total energy for LP (with 10% and 14% being the contributions of ions emitted from the front and rear sides, respectively) and almost 100% for CP.

The reason why the “ponderomotive” peak in the ion energy spectrum is much more prominent for CP than for LP is attributed to the fact that the ponderomotive force tends to focus the ion spatially at the end of the skin layer, creating a very sharp density peak.^{18,19} For LP, the strong electron pressure counteracts the piling up of the ions, leading to “explosion” of the proton bunch and to a broader energy spectrum; the maximum ion energy is higher for LP than for CP, as a few of the ponderomotively accelerated ions gain additional energy

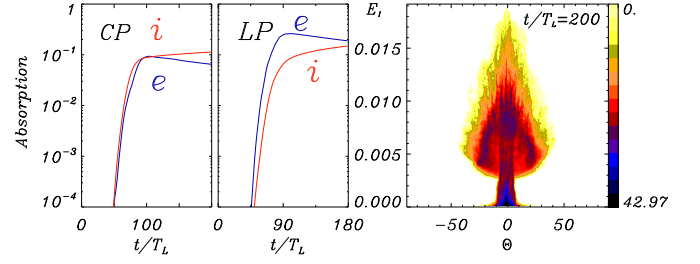


FIG. 3: 2D simulation results. Left: comparison of absorption efficiency into ions and electrons vs. time. Right: energy vs. angle distribution of ions. The pulse radius is $r_L = 2 \mu\text{m}$. Other parameters are the same of the 1D runs of Figs.1-2.

from the fast electrons. The comparison with the CP simulation shows that in this latter case it is the relatively low electron temperature which allows for a narrow ion energy spectrum.

The comparison of 1D, plane-wave simulations best enlightens the different regimes of ion acceleration between LP and CP and the particular features of PA vs. TNSA. For a realistic laser pulse with a finite spot size, the differences between LP and CP are somewhat weakened by the effects of pulse focusing which introduces electric field components normal to the target surface at the edges of the spot, leading to electron heating. Fig.3 shows the effect on fractional absorption in 2D simulations with the same parameters of the 1D case, and a tightly focused pulse with a spot radius $r_L = 2\lambda_L$. The differences between LP and CP and between ion and electron absorption in the latter case are less dramatic as expected, but still substantial.

The angular spread of ions depends upon their energy E . The $f(E, \Theta)$ distribution of ions in [Fig.3 b)], where Θ is the emission angle with respect to the target normal shows that the most energetic the ions the most collimated they are: for instance, ions having energy exceeding $0.01m_i c^2$ are found within a cone with an aperture angle of about 10 degrees. Wider spot sizes or smoother intensity profiles may yield a lower divergence.

The narrow ion energy spectrum of the CP case is a necessary condition to obtain a dense ion bunch with very short duration, in addition to the requirement of a laser pulse with duration of the order of the bunch acceleration time.¹⁸ These particular features of ions accelerated using CP pulses may be useful for ultrafast, localized energy deposition in matter, and are essential for a proposed concept of sources of fusion neutrons with duration of a few femtoseconds.²⁰

The production of a single, ultrashort ion bunch can be observed in the simulation of Fig.4 (for which $I = 5.5 \times 10^{18} \text{ W cm}^{-2}$, $\tau_L = 33 \text{ fs}$ and $r_L = 4 \mu\text{m}$) where, in addition, a linear density profile was used instead of a step-like one to address the effect of early plasma production by a prepulse in experiments. We observe that ion acceleration initially occurs near the cut-off layer where $n_e = n_c$, and produces at $t \simeq 30T_L$ a narrow ion bunch

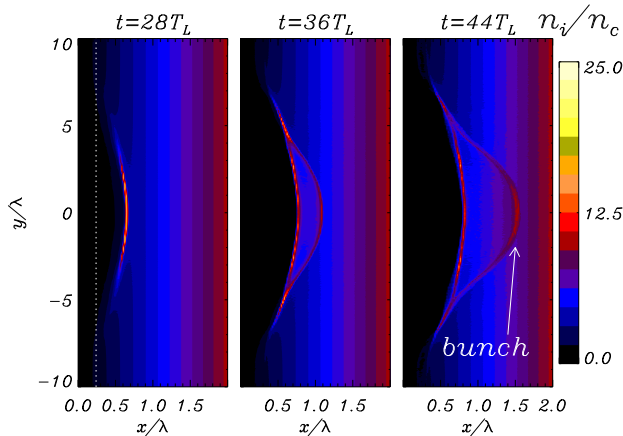


FIG. 4: Snapshots of ion density from a 2D, CP simulation for a linear density profile rising from 0 to $10n_c$ over 2λ . Laser pulse parameters are $a_L = 2$, $\tau_L = 10T_L$ and $r_L = 4\lambda$. The white dotted line indicates the initial position of the $n_e = n_c$ surface. The arrow indicates the location of the short ion “bunch” at $t = 44T_L$.

with a density larger than $10n_c$. The divergence of the bunch ions is about 4 degrees.

So far, laser-plasma interaction experiments with CP have been rarely reported. Kado et al.²¹ observed a collimated proton beam in the interaction of CP pulses with plastic-coated Tantalum targets at an intensity of $4 \times 10^{18} \text{ W cm}^{-2}$. In addition, no electrons with energy beyond 20 keV were observed in these conditions.²² These observations are in qualitative agreement with the above scenario of CP laser ion acceleration. Fukumi et al.²³ also reported ion energy measurements for a CP laser pulse but, since a substantial incidence angle (45 deg) was used, the interaction conditions were rather similar to an overlap of *s*- and *p*-polarized laser pulses, causing a dominant effect of electron heating and TNSA of ions. Since no unaffordable problem seems to prevent the use of high-intensity CP pulses at normal incidence for laser-plasma interactions, the regime of ion acceleration with CP pulses may be investigated in present-day experiments allowing progress in the use of laser-accelerated ions for specific applications.

This work has been supported by the Italian Ministry for University and Research (MIUR) via the PRIN project “Ultraintense laser-plasma interaction”, by CNR-INFM and CINECA (Italy) through the super-computing initiative, and by JSCC (Moscow, Russia).

* On leave from Institute for Computational Technologies, SD-RAS, Novosibirsk, Russia

† Electronic address: macchi@df.unipi.it

¹ J. A. Cobble, R. P. Johnson, T. E. Cowan, N. R.-L. Galoudec, and M. Allen, *J. Appl. Phys.* **92**, 1775 (2002).

² A. J. MacKinnon, P. K. Patel, D. W. Price, D. Hicks, L. Romagnani, and M. Borghesi, *Appl. Phys. Lett.* **82**, 3188 (2003).

³ M. Borghesi, L. Romagnani, A. Schiavi, D. H. Campbell, M. G. Haines, O. Willi, A. J. MacKinnon, M. Galimberti, L. Gizzi, R. J. Clarke, S. Hawkes, *Appl. Phys. Lett.* **82**, 1529 (2003).

⁴ C. K. Li, F. H. Seguin, J. A. Frenje, J. R. Rygg, R. D. Petrasso, R. P. J. Town, P. A. Amendt, S. P. Hatchett, O. L. Landen, A. J. MacKinnon, P. K. Patel, V. A. Smalyuk, T. C. Sangster, J. P. Knauer, *Phys. Rev. Lett.* **97**, 135003 (2006).

⁵ P. K. Patel, A. J. MacKinnon, M. H. Key, T. E. Cowan, M. E. Foord, M. Allen, D. F. Price, H. Ruhl, P. T. Springer, and R. Stephens, *Phys. Rev. Lett.* **91**, 125004 (2003).

⁶ K. Nemoto, A. Maksimchuk, S. Banerjee, K. Flippo, G. Mourou, D. Umstadter, and V. Y. Bychenkov, *Appl. Phys. Lett.* **78**, 595 (2001).

⁷ P. McKenna, K. E. D. Ledingham, T. McKanny, R. P. Singhal, I. Spencer, E. L. Clark, F. N. Beg, K. Krushelnick, M. S. Wei, J. Galy, J. Magill, R. J. Clarke, K. L. Lancaster, P. A. Norreys, K. Spohr, R. Chapman, *Appl. Phys. Lett.* **83**, 2763 (2003).

⁸ V. Malka, S. Fritzler, E. Lefebvre, E. d’Humières, R. Ferland, G. Grillon, C. Albaret, S. Meyroneinc, J. P. Chambaret, A. Antonetti, D. Hulin, *Med. Phys.* **31**, 1587 (2004).

⁹ S. Atzeni, M. Temporal, and J. J. Honrubia, *Nucl. Fusion*

42, L1 (2002).

¹⁰ F. Terranova, S. V. Bulanov, J. L. Collier, H. Kiriyaama, and F. Pegoraro, *Nucl. Inst. Meth. Phys. Res. A* **558**, 430 (2006).

¹¹ B. M. Hegelich, B. J. Albright, J. Cobble, K. Flippo, S. Letring, M. Paffett, H. Ruhl, J. Schreiber, R. K. Schulze, and J. C. Fernandez, *Nature* **439**, 441 (2006).

¹² H. Schwoerer, S. Pfotenhauer, O. Jaekel, K. U. Amthor, B. Liesfeld, W. Ziegler, R. Sauerbrey, K. W. D. Ledingham, and T. Esirkepov, *Nature* **439**, 445 (2006).

¹³ T. Toncian, M. Borghesi, J. Fuchs, E. d’Humières, P. Antici, P. Audebert, E. Brambrink, C. A. Cecchetti, A. Pipahl, L. Romagnani, O. Willi, *Science* **312**, 410 (2006).

¹⁴ S. C. Wilks, A. B. Langdon, T. E. Cowan, M. Roth, M. Singh, S. Hatchett, M. H. Key, D. Pennington, A. MacKinnon, and R. A. Snavely, *Phys. Plasmas* **8**, 542 (2001).

¹⁵ L. O. Silva, M. Marti, J. R. Davies, R. A. Fonseca, C. Ren, F. S. Tsung, and W. B. Mori, *Phys. Rev. Lett.* **92**, 015002 (2004).

¹⁶ T. Esirkepov, M. Borghesi, S. V. Bulanov, G. Mourou, and T. Tajima, *Phys. Rev. Lett.* **92**, 175003 (2004).

¹⁷ J. Badziak, S. Jablonski, and S. Glowacz, *Appl. Phys. Lett.* **89**, 061504 (2006).

¹⁸ A. Macchi, F. Cattani, T. V. Liseykina, and F. Cornolti, *Phys. Rev. Lett.* **94**, 165003 (2005).

¹⁹ Y. Sentoku, T. E. Cowan, A. Kemp, and H. Ruhl, *Phys. Plasmas* **10**, 2009 (2003).

²⁰ A. Macchi, *Appl. Phys. B: Laser and Optics* **82**, 337 (2006).

²¹ M. Kado, H. Daido, A. Fukumi, Z. Li, S. Orimo, Y. Hayashi, M. Nishiuchi, A. Sagisaka, K. Ogura, S. Nakamura, A. Noda, Y. Iwashita, T. Shirai, H. Tongu,

- T. Takeuchi, A. Yamazaki, H. Itoh, H. Souda, K. Nemoto, Y. Oishi, T. Nayuki, H. Kiriya, S. Kanazawa, M. Aoyama, Y. Akahane, N. Inoue, K. Tsuji, Y. Nakai, Y. Yamamoto, H. Kotaki, S. Kondo, S. Bulanov, T. Esirkepov, T. Utsumi, A. Nagaschima, T. Kimura, K. Yamakawa, *Las. Part. Beams* **24**, 117 (2006).
- ²² H. Daido, private communication.
- ²³ A. Fukumi, M. Nishiuchi, H. Daido, Z. Li, A. Sagisaka, K. Ogura, S. Orimo, M. Kado, Y. Hayashi, M. Mori, S. V. Bulanov, T. Esirkepov, K. Nemoto, Y. Oishi, T. Nayuki, T. Fujii, A. Noda, S. Nakamura, *Phys. Plasmas* **12**, 100701 (2005).